Applied Catalysis A, General 542 (2017) 296–305

Contents lists available at ScienceDirect

Applied Catalysis A, General

journal homepage: www.elsevier.com/locate/apcata

# In-situ XANES and XPD studies of $NiO/Ce_{0.9}Zr_{0.1}O_2$ IT-SOFCs anode nanomaterial as catalyst in the CPOM reaction

M.G. Zimicz[a,*], F.D. Prado[a], D.G. Lamas[b], S.A. Larrondo[c,d]

[a] Departamento de Física, Universidad Nacional del Sur, and Instituto de Física del Sur, CONICET, Av. L.N. Alem 1253, 8000 Bahía Blanca, Pcia. de Buenos Aires, Argentina

[b] CONICET and Universidad Nacional de Gral. San Martín, Escuela de Ciencia y Tecnología, Campus Miguelete, Edificio Tornavías, 25 de Mayo y Francia, 1650 San Martín, Pcia. de Buenos Aires, Argentina

[c] UNIDEF, MINDEF, CONICET, Departamento de Investigaciones en Sólidos, CITEDEF, Juan. B. de La Salle N°4397, 1603 Villa Martelli, Pcia. de Buenos Aires, Argentina

[d] Instituto de Investigación e Ingeniería Ambiental, Universidad Nacional de Gral. San Martín, Campus Miguelete, 25 de Mayo y Francia, 1650 San Martín, Pcia. de Buenos Aires, Argentina

ARTICLE INFO

*Keywords:*
In situ XANES
in situ XPD
Methane catalytic oxidation
Mass spectrometry

ABSTRACT

The aim of this paper is to study the oxidation states of metal cations and the changes in the crystalline phases in $NiO/Ce_{0.9}Zr_{0.1}O_2$ nanocatalysts under typical conditions of methane catalytic partial oxidation reaction by in-situ X ray absorption near edge spectroscopy (XANES) and X-ray powder diffraction (XPD) studies. The $Ce_{0.9}Zr_{0.1}O_2$ mixed oxide was obtained by glycine-nitrate-combustion method, being the nickel incorporated by incipient wetness impregnation. The evolution of the crystalline structure with temperature and operating conditions was followed by in-situ XPD experiments and the oxidation states of Ce and Ni cations by in-situ XANES experiments at the Ce-$L_{III}$ and Ni-K absorption edges. It was observed that NiO is completely reduced to Ni° at temperatures above 650 °C while $Ce_{0.9}Zr_{0.1}O_2$ fluorite-like phase showed changes in lattice parameter due to cerium reduction and crystallite growth, but no phase transformations or segregations were observed. It was confirmed that Ni° is the active centre to activate methane molecule while $Ce^{4+}/Ce^{3+}$ ratio is strongly related with $CO/CO_2$ concentration in the exhaust gas flow.

## 1. Introduction

The development of the global economy has led to intensive use of fossil fuels, with a consequent increase in environmental pollution and emissions of greenhouse gases. The concern about the level of air pollution and global warming has given great impulse to the development of more efficient and cleaner energy production technologies. The utilization of renewable sources of energy and the development of sustainable processes are key issues in the energy economy. In this context, the energy production from biomass [1], solar cells [2], and fuel cells [3] are some of the main subjects in current investigations seeking to contribute to the solution of environmental pollution. Among the different types of fuel cells under development, solid oxide fuel cells (SOFCs) show great advantages over the others, due to the possibility of feeding the cells with fossil fuels like methane. SOFCs present better performance when operating with synthesis gas instead of methane, due to the faster electro-oxidizing of CO and $H_2$. In the high-temperature SOFCs operating at temperatures above 900 °C, synthesis gas is obtained by methane reforming in the anode or an external chamber. This method is not efficient enough when applied in intermediate-temperature SOFCs (IT-SOFCs) that operate in the 500 °C–800 °C temperature range. One of the possibilities to increase the performance of methane-fueled IT-SOFCs is to convert methane to synthesis gas by catalytic partial oxidation (CPOM). This reaction can be described by the following equation:

$$CH_4(g) + 0.5O_2(g) \Rightarrow 2\,H_2(g) + CO(g)\ \Delta H^0 = -36\ kJ/mol$$

Noble metals like Rh, Ru, Pt and Pd are catalysts very active for this reaction, showing a direct conversion mechanism of methane into synthesis gas without the appearance of carbon deposits [4–9]. However, the use of these high cost and low availability metals is totally discouraged in the development of cleaner and more efficient energy production systems. Cheaper transition metals, especially nickel, are preferred to catalyze this reaction with lower costs. In this regard, the use of $CeO_2$-based oxides as nickel phase support prevents accumulation of carbon deposits on the surface of the catalyst helping to maintain the level of activity [10].

Many researchers have studied ceria-based supports for CPOM

* Corresponding author.
*E-mail addresses:* mgzimicz@ifisur-conicet.gov.ar, geno.zimicz@gmail.com (M.G. Zimicz).

http://dx.doi.org/10.1016/j.apcata.2017.05.040
Received 20 March 2017; Received in revised form 19 May 2017; Accepted 26 May 2017

reaction with nickel catalysts [11–15]. In this work, $CeO_2$-$ZrO_2$ was selected as support based on the better reducibility and oxygen storage capacity observed in Zr-doped ceria. Among the different Zr contents that could be reached in the $Ce_xZr_{1-x}O_d$ system, those corresponding to $x < 0,5$ showed the better redox behavior. Nevertheless, the compositions in that region are metastable and some decomposition due to aging should be expected. Samples corresponding to the cerium rich region ($x > 0.8$) are thermodynamically stable with good reducibility an oxygen availability [16–18].

In this context, the Ni° particle size and the interaction with the support are critical aspects that affect the catalyst performance [13]. Pre-reduction of nickel phase produces better catalyst performance, which was attributed to re-dispersion of metallic particles or better interaction with the support [11].

In this sense, Pal et al. [15] have recently reported the development of Ni/CeO2 catalyst with an optimized Ni content of 7.5 wt%, yielding a methane conversion of 98% at 800 °C with no observable deactivation after 50 h of time-on-stream. They believe that formation of the Ce—O—Ni—O— layer with under-coordinated oxygen atoms on the surface may be responsible of the catalytic activity levels and good performance reached. Pantaleo et al. [19] have reported the analysis of 6 wt% Ni/$CeO_2$ catalyst. They affirm that the crystallite sizes and the interaction between NiO and $CeO_2$, which is controlled by varying the catalyst preparation procedure, are determinant factors for the activity and stability during the partial oxidation of methane. They did not observe deactivation of the catalyst and reported methane conversion of 90% at 650 °C over pre-reduced Ni/$CeO_2$. We have previously reported the catalytic performance of NiO/$Ce_{0.9}Zr_{0.1}O_2$ catalysts in total and partial oxidation of methane [20,21]. In this catalyst the Ni phase was incorporated by incipient wetness impregnation of the support. The positive influence of the high oxygen mobility of the $Ce_{0.9}Zr_{0.1}O_2$ support in the catalyst stability was observed [20]. Besides, we found that the NiO(60 wt.%)/$Ce_{0.9}Zr_{0.1}O_2$ cermet was an excellent anode material for IT-SOFCs [21,22]. The Ni° content should be greater than ~30 vol. %, in order to provide a good electronic conductivity. A Ni° content of 50 vol.% is generally preferred, which is equivalent to a 60 wt.% of NiO [23].

Based on the previous information, it is worth to get a deep insight of the evolution of crystallite size, the stability of crystalline structure and the modification of the oxidation states of cerium and nickel cations of this anode material when it is exposed to atmospheres containing methane and oxygen in the temperature range used in IT-SOFCs. Besides, it seeks to establish some relationship between structural and metal cation oxidation states with product distribution in the reactor effluent.

Therefore, in this paper we study the crystallite size and the structure by in-situ X-ray powder diffraction (XPD), and the oxidation states of Ce and Ni cations by in-situ XANES experiments at the Ce-$L_{III}$ and Ni-K absorption edges. The experiments were performed with synchrotron radiation in an extended temperature range and with different feed gas-flowcompositions. Mass spectrometry data were collected during in-situ tests in order to observe the species present at the exit of the reactor. The results of these experiments are analyzed and compared with those obtained in conventional catalytic tests conducted in a fixed-bed laboratory reactor.

## 2. Experimental

### 2.1. Synthesis

$Ce_{0.9}Zr_{0.1}O_2$ mixed oxide support was synthesized by the stoichiometric glycine-nitrate combustion route, starting from $ZrO(NO_3)_2{\cdot}6H_2O$ (Fluka, Zr 27 wt.%), $Ce(NO_3)_3{\cdot}6H_2O$ (Alfa Aesar, 99,95%) and glycine (Merck, > 98.5%). The synthesis process was described elsewhere [24]. The as-obtained solids were calcined at 600 °C in air in order to eliminate any vestige of carbonaceous residues. This support will be referred to hereinafter as ZDC. Ni was incorporated to the ZDC support by incipient wetness impregnation of alcoholic $Ni(NO_3)_2{\cdot}6H_2O$ solution of suitable concentration, in order to get a NiO nominal content of 60 wt. % in the final catalyst. After impregnation, the solids were dried at 90 °C and calcined at 350 °C for 2 h in order to convert all the nickel into NiO. A subsequent thermal treatment at 1000 °C for 2 h was performed in order to simulate the conditions used in the construction of the IT-SOFC. The obtained NiO/$Ce_{0.9}Zr_{0.1}O_2$ cermet will be referred to hereinafter as NiO/ZDC.

### 2.2. Conventional characterization studies

#### 2.2.1. Conventional X-ray powder diffraction (XPD)

Conventional X-ray powder diffraction (XPD) patterns were recorded with a Phillips PW3710 diffractometer using CuKα radiation, equipped with a graphite monochromator and operated at 40 kV and 30 mA. Data were collected in the $2\theta = 20°–100°$ region, with a step-size of 0.02° and a step-counting time of 12 s.

#### 2.2.2. $N_2$ physisorption

Physisorption of nitrogen at its normal boiling point was performed with a Quantachrome Autosorb-1 to evaluate total pore volume and specific surface area using the five points BET method. Prior to the measurements, the samples were degassed at 250 °C for 7 h under vacuum (pressure < 20 mmHg).

#### 2.2.3. SEM

The morphology and chemical composition of the powders were studied by scanning electron microscopy (SEM) employing a Zeiss Supra 40 microscope, equipped with an energy dispersive X-ray spectrometer (EDS). The accelerating voltage was 5 kV.

### 2.3. In-situ XPD tests with synchrotron light

Time-resolved diffraction data were collected at the D10B-XPD beamline facility of the Brazilian Synchrotron Light Laboratory (LNLS, Campinas, Brazil: Proposal XRD1-14413) using a high-intensity and low-resolution configuration, without crystal analyzer. The energy was set at 8 keV and the X-ray wavelength was 1.5498 Å. The peak profile was not significantly affected by low resolution since peaks are intrinsically broad due to the nanometric crystallite size. The powders were placed in the sample-holder provided with a thermocouple to read the sample temperature during the experiments. The set up allows putting the sample inside a reactor with controlled heating and gas-flow lines. The inlet line is connected to a gas-mixing station equipped with mass flow controllers to set $H_2$:He or $CH_4$:$O_2$:He gas-flow compositions. The outlet line is connected to a Pfeiffer QMS 422 Quadrupole Mass Spectrometer to follow the composition of the exit gas flow. Rietveld refinement of diffraction patterns were performed using the Full Prof Suite open access software [25].

### 2.4. In-situ XANES experiments with synchrotron light

These experiments were performed for Ce $L_{III}$ and Ni K edges. These tests were carried out in the D06A-DXAS beam-line facility of the Brazilian Synchrotron Light Laboratory (LNLS, Campinas, Brazil: Proposal DXAS-9949). The samples were prepared by mixing NiO/ZDC powder with boron nitride, an inert and weak absorbing binder in the energy band of the experiments, in an adequate proportion to give a total absorption ratio of about 1.5. The mixture was pressed into discs and placed in a sample-holder which is introduced in a quartz tubular reactor having inlet and outlet gas lines. The inlet line is connected to a gas-mixing station equipped with mass flow controllers and the outlet line is connected to a Pfeiffer QMS 422 Quadrupole Mass Spectrometer. XANES spectra were collected in transmission mode at the Ce $L_{III}$-edge and Ni K-edge with different $H_2$:He or $CH_4$:$O_2$:He gas-flow compositions

over the temperature range 20 °C to 800 °C. Linear combination of standard spectra was used to evaluate the reduction percentage of the different cations as it was previously reported [26].

During the experiments performed with diluted $H_2$, the catalyst was heated at 10 °C $min^{-1}$ from room temperature to 550 °C with a dwell time of 30 min at 550 °C, in a flow consisting of 5 v/v% $H_2$ (He balance). The selected final temperature is 200 °C above the 350 °C used in the catalyst pre-treatment in order to see the characteristics of the full reduction of NiO. XRD patterns were collected in the 2θ = 36°–47° angular range, with a typical collecting time of 2–3 min.

### 2.5. Catalytic tests in conventional fixed-bed reactor

Catalytic tests were carried out in a laboratory fixed-bed reactor, operated isothermally at atmospheric pressure. The feed consisted of a mixture of 2% $CH_4$, 1% $O_2$ and $N_2$ balance, with a total flow of 333 $cm^3$ (NPTC) $min^{-1}$. Feed and effluent compositions were determined by on-line gas chromatography in a Clarus 500 Perkin Elmer chromatograph. The catalyst mass was 100 mg in all experiments, and the catalytic bed was diluted with inert material in a 6:1 mass ratio, in order to avoid the presence of hot spots. Preliminary catalytic tests were performed to ensure negligible contribution of homogeneous phase reaction, no contribution of inert material to conversion and the absence of diffusional intra and inter particles limitations.

A pre-reduction treatment was performed just before the catalytic tests, with a continuous flow of 200 $cm^3$(NPTC) $min^{-1}$ containing 7 mol% $H_2$ ($N_2$ balance) at a temperature of 350 °C for 2 h. Methane conversion and selectivity to CO and $CO_2$ were calculated as:

$$X_{CH_4} = \frac{(F^i_{CH_4} - F^o_{CH_4})}{F^i_{CH_4}} 100\%$$

$$S_{CO} = \frac{F^o_{CO}}{(F^i_{CH_4} - F^o_{CH_4})} 100\%$$

$$S_{CO_2} = \frac{F^o_{CO_2}}{(F^i_{CH_4} - F^o_{CH_4})} 100\%$$

where $F^i_k$ and $F^o_k$ represent the molar flow of component *"k"* in the reactor inlet and outlet, respectively.

## 3. Results and discussion

### 3.1. Conventional characterization studies

In Fig. 1, conventional XPD patterns of ZDC and fresh and spent samples of NiO/ZDC are plotted. ZDC support (Fig. 1(a)) shows the Bragg peaks corresponding to the fluorite-type crystal structure, while sample NiO/ZDC before the catalytic tests (Fig. 1(b)) shows the characteristic NiO peaks superimposed with those corresponding to ZDC support, indicating that NiO is in a separated phase. The XPD patterns of NiO/ZDC spent catalyst tested with a feed ratio $CH_4$:$O_2$ = 2 (Fig. 1(c)) exhibit the presence of the more intense Ni° diffraction peaks with no observation of NiO, indicating that NiO was totally reduced to Ni° during the reaction process. Likewise, it is observed a new Bragg peak centered on 2θ = 26° corresponding to graphitic carbon (according the ICSD #52230) indicating the formation of carbonaceous deposits during the experiments. However, sample tested in methane oxidation in conventional fixed-bed reactor, with a feed ratio $CH_4$:$O_2$ = 1 (Fig. 1(d)), exhibited the presence of Ni° and NiO. It should be mentioned that the diffraction patterns of spent samples were collected in ambient air, so reoxidation by atmospheric air cannot be discarded.

The average crystallite size was estimated from the width of the (111) peak centered at 2θ = 28.7° using the Scherrer equation, $D = 0.9\lambda b^{-1}[Cos(\theta)]^{-1}$, where D is the crystallite size, λ is the radiation wavelength, β is the corrected peak width at half-maximum intensity and θ is the peak angular position. Average crystallite sizes, specific surface area (A) and pore volume (V) for samples ZDC and NiO/ZDC are summarized in Table 1. There is a drastic reduction of the specific surface of ZDC support after impregnation with NiO and calcination at 1000 °C (sample NiO/ZDC), due to sintering processes in both nickel and ceria based solid phases.

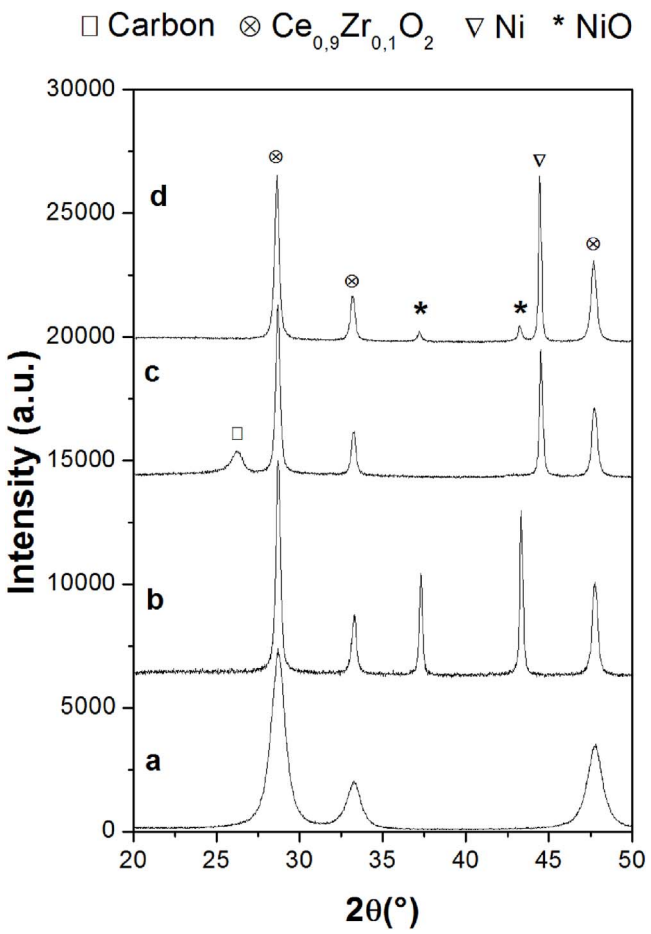


**Fig. 1.** Diffraction patterns of: (a) ZDC support after calcination at 600 °C; (b) NiO/ZDC heat treated at 1000 °C; (c) NiO/ZDC spent catalyst after CPOM reaction in fixed bed reactor in $CH_4$:$O_2$ = 2 and (d) $CH_4$:$O_2$ = 1.

**Table 1**
Morphological properties of samples ZDC and NiO/ZDC.

| Sample | Calcination temperature (°C) | D of ZDC crystallites (nm) | A ($m^2$/g) | V ($cm^3$/g) |
|---|---|---|---|---|
| ZDC | 600 | 8.6 (4) | 45 (2) | 0.086 (4) |
| NIO/ZDC | 1000 | 38 (1) | 7.2 (1) | 0.0036 (2) |

In Fig. 2, SEM images of fresh and spent catalysts are presented. Sample ZDC (Fig. 2(a)) has a porous structure which favors the access of gas flow accessing to the catalyst surface. However, after impregnation with NiO (Fig. 2(b)) and calcination at 1000 °C the structure loses some porosity due to crystallite growth induced by high temperature. The Fig. 2(c), corresponding to the catalyst NiO/ZDC after catalytic test at 700 °C in $CH_4$:$O_2$ = 2, shows the presence of filaments evidencing carbon deposition during reaction. In Fig. 2(d), it can be seen that there is no formation of carbonaceous deposits over NiO/ZDC after test in $CH_4$:$O_2$ = 1. All these observations are in agreement with XPD analysis (Fig. 1). This result evidences the importance of an equilibrium between methane dehydrogenation, the oxidation of carbon filaments by oxygen from the laticce of ceria based oxide, and the interaction between nickel and ceria-based support.

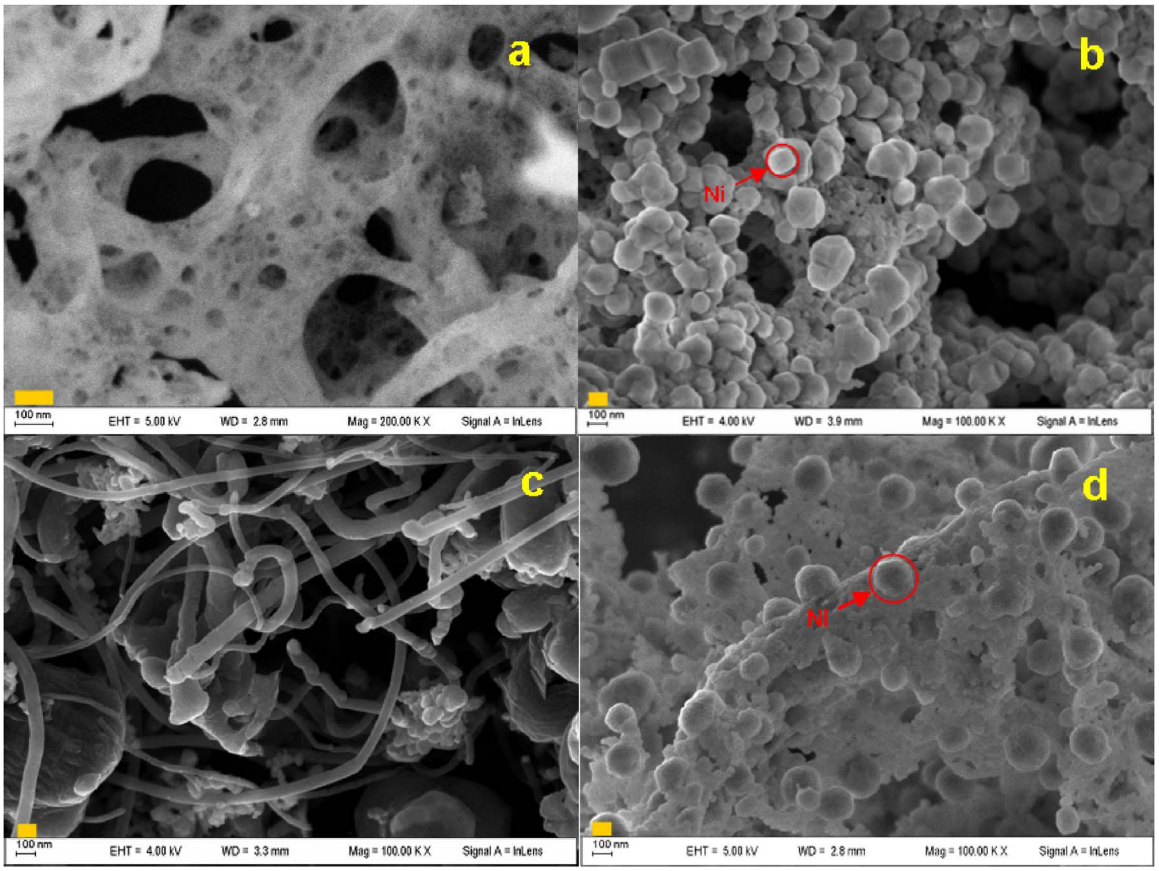


**Fig. 2.** SEM images of: (a) ZDC support calcined at 600 °C, (b) NiO/ZDC fresh catalyst calcined at 1000 °C and (c) NiO/ZDC spent catalyst after CPOM reaction with a feed ratio $CH_4$:$O_2$ = 2 and (d) $CH_4$:$O_2$ = 1. Yellow bar at the left bottom of each micrograph represent 100 nm. (For interpretation of the references to color in this figure legend, the reader is referred to the web version of this article.)

Average chemical composition obtained from EDS (Energy-dispersive X-Ray spectroscopy) mapping analysis gave a composition of 61 wt.% of NiO and 39 wt.% of $Ce_{0.9}Zr_{0.1}O_2$ for sample NiO/ZDC (NiO (60 wt.%)/$Ce_{0.9}Zr_{0.1}O_2$) which is in excellent agreement with the nominal value.

EDS results for spent NiO/ZDC sample after the catalytic test at 700 °C in $CH_4$:$O_2$ = 2:1 presented 69 wt.% of carbon. In the rest of the samples carbon was not detected.

### 3.2. *In situ characterization techniques with synchrotron light during pre-reduction treatment*

#### 3.2.1. *In situ XPD experiments*

In these in situ XPD experiments we follow the NiO→Ni° reduction occurring during the pre-reduction treatment performed over the fresh catalysts prior to the catalytic experiments. We began analyzing the diffraction pattern of the catalyst at the beginning of the experiment in order to determine the initial crystallographic characteristics. It was observed the presence of only two phases, the ZDC support and the NiO impregnated phase. The outcoming composition obtained from quantitative phase analysis by Rietveld refinement was 39 wt.% of ZDC phase and 61 wt.% of NiO, values totally compatible with the nominal composition of NiO/ZDC (60 wt.%NiO/40 wt.% ZDC) and in agreement with EDS results. After that, the sample was exposed to a gas flow of 50 $cm^3$(CNPT) $min^{-1}$ consisted of 5 v/v% $H_2$ in He. The catalyst was heated at 10 °C/min from 20 °C to 350 °C, with a dwell time of 2 h at 350 °C.

Fig. 3 presents a selection of the more significant diffraction patterns. When the sample reaches 350 °C, nickel is still present as NiO. After 25 min at this temperature the main Bragg peaks of Ni° appeared,

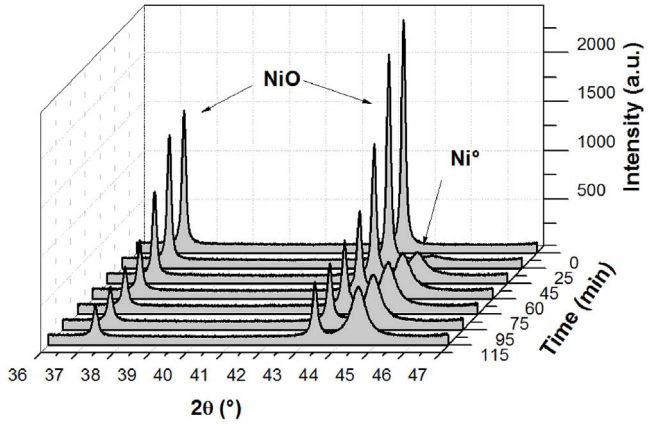


**Fig. 3.** XRD patterns collected during the pre-reduction treatment of NiO/ZDC; feed composition of 5 v/v% $H_2$ in He gas flow at T = 350 °C.

indicating the direct conversion of NiO to Ni° without the appearance of intermediate phases ($NiO_x$). The proportion of Ni° increases with time at the expense of decreased NiO signals. At the end of the pre-treatment, NiO and $Ni^0$ coexist in the sample.

In Fig. 4a, the evolution of the reduction percentage after reaching 350 °C is depicted. The reduction curve is sigmoidal, with an induction period with low reduction kinetic, and an accelerated process after a certain critical time (approximately 20 min), corresponding to the nucleation kinetic model [27].

The final reduction percentage reached after two hours at 350 °C is 90%. It is worth to mention that NiO reduction is a very complex process, dependent of many variables, like NiO grain size, the

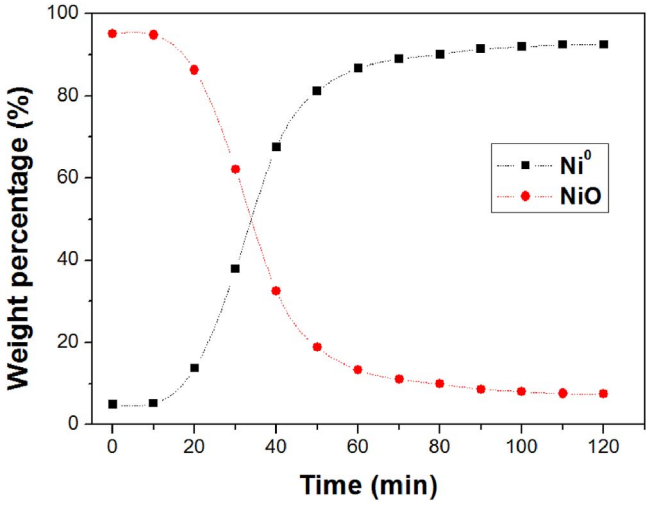


**Fig. 4.** Evolution of the nickel reduction percentage during reduction of sample NiO/ZDC in 5 v/v% $H_2$ at 350 °C.

interaction with the support and the presence of oxygen vacancies in the surface [27]. In order to have a better understanding of the reduction process of supported NiO XANES studies were performed in the Ni K edge.

### 3.2.2. *In situ XANES experiments in the Ni K-edge*

The degree of reduction of NiO was obtained as a linear combination of Ni° and NiO XANES spectra standards (Fig. 5). Fig. 6 shows the evolution of the degree of reduction with temperature and the corresponding spectra collected in atmosphere of 5 v/v% $H_2$ in He.

As it was described in the previous sub-section, the reduction process starts at 350 °C with an induction period showing very low rate until reaching 450 °C. At higher temperatures reduction rate increases rapidly reaching 100% of reduction at 550 °C. This suggests that in order to completely reduce the NiO it is necessary to operate at temperatures above 450 °C where the kinetics increases dramatically.

### 3.3. *In situ characterization techniques with synchrotron light during catalytic tests*

### 3.3.1. *In situ XPD experiments*

After the pre-treatment with hydrogen at 350 °C previously described, we performed catalytic tests in 2 v/v% $CH_4$ −1 v/v% $O_2$ (He balance) feed gas flow. In this case, the samples were heated at 10 °C/min from 350 °C up to 750 °C, with isothermal steps of 30 min at

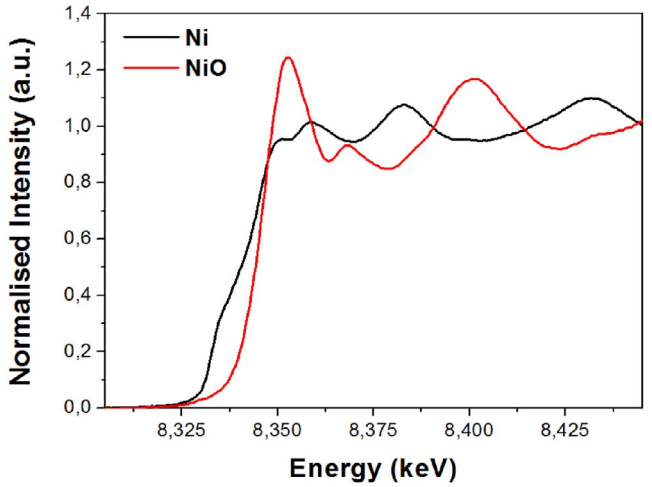


**Fig. 5.** XANES spectra at the Ni K-edge for Ni and NiO standards.

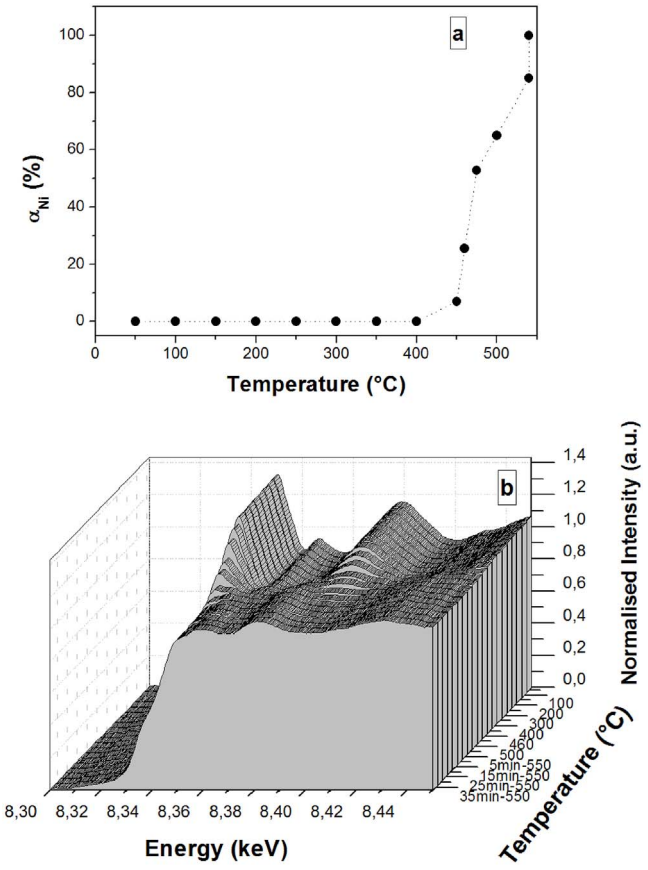


**Fig. 6.** a) Evolution of degree of reduction of $Ni^{2+}$ with temperature in 5 v/v% $H_2$; b) XANES spectra collected during the reduction process in 5 v/v% $H_2$ (He balance) from ambient temperature up to 550 °C.

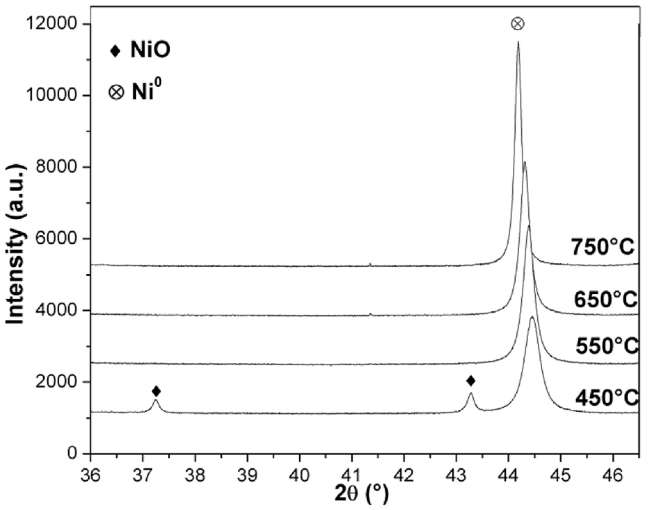


**Fig. 7.** Diffraction patterns collected at isothermal steps during CPOM for pre-reduced NiO/ZDC. Feed composition: 2 v/v% $CH_4$ −1 v/v% $O_2$ (He balance).

450 °C, 550 °C, 650 °C, and 750 °C. Diffraction patterns were collected during the isothermal periods (see Fig. 7). From XRD data it is possible to evaluate the evolution of catalyst composition, crystallite size and carbon deposition of the catalytic system during the catalytic tests.

Regarding the nickel oxidation state, as it was said in a previous paragraph, nickel coexists as NiO and $Ni^0$ (~10% and 90% respectively) after the pre-reduction process. The Rietveld refinement of diffraction patterns of the sample in the reaction atmosphere at 450 °C gives a composition of 9 wt.% NiO, 47 wt.% Ni and 44 wt.% ZDC (16%

**Table 2**
Rietveld refinement results of XPD patterns collected during CPOM.

| Temperature (°C) | $a_{ZDC}$ (Å) | $a_{NiO}$ (Å) | $a_{Ni}$ (Å) |
|---|---|---|---|
| 25 | 5.388 (1) | 4.177 (1) | – |
| 450 | 5.423 (1) | 4.205 (1) | 3.550 (1) |
| 550 | 5.438 (1) | – | 3.558 (1) |
| 650 | 5.454 (1) | – | 3.564 (1) |
| 750 | 5.487 (1) | – | 3.572 (1) |

of NiO, 84% of $Ni^0$). These values indicate that some reoxidation of Ni took place due to the presence of oxygen in the gas flow. Finally, at 550 °C NiO is no longer detected. Instead, only Ni° and ZDC phases are identified. Rietveld refinement gives a composition of 54 wt.% Ni° and 46 wt.% ZDC.

There is no evidence of carbon deposition during the catalytic tests performed in these experiments, being this result against our observations in the fixed bed experiments. This difference can be attributed to the lower space time (catalyst mass to gas flow ratio) used in these experiments with synchrotron light, at the XPD line. The evolution with temperature of lattice parameters of the cubic structure of ZDC, NiO and Ni is summarized in Table 2. The Rietveld results of the fresh catalyst at 25 °C are reported for comparison purposes.

It can be seen that the lattice parameter increases with increasing temperature. This result suggests that some $Ce^{4+}$ cations of the ZDC lattice were reduced to $Ce^{3+}$ with the associated increment of the ionic radius (0.97 Å for $Ce^{4+}$ and 1.14 Å for $Ce^{3+}$) [28] contributing to the lattice parameter growth. In situ XPD experiments performed over a ZDC sample at 750 °C in 5 v/v% $H_2$ (He balance) and synthetic air atmospheres, showed that the lattice parameter of sample heated in air is lower than that observed in reducing atmosphere (5.441 Å and 5.461 Å respectively), indicating that the increment in lattice parameter presented in Table 2 is not only due to thermal expansion, but also to the reduction of $Ce^{4+}$ cations.

Similar XPD analyses during catalytic tests in 2 v/v% $CH_4$ −1 v/v% $O_2$ (He balance) feed gas flow were performed over NiO/ZDC sample without pre-reduction treatment, and the results are presented in Fig. 8. Up to 650 °C only NiO is present in the sample, and above this temperature NiO is completely reduced to $Ni^0$. Therefore, without pre-treatment the necessary presence of Ni° to obtain synthesis gas is achieved at higher temperatures. This reduction process will be faster than that developed in the pre-treatment but, on the other hand, larger Ni° particles could be obtained due to the higher temperatures.

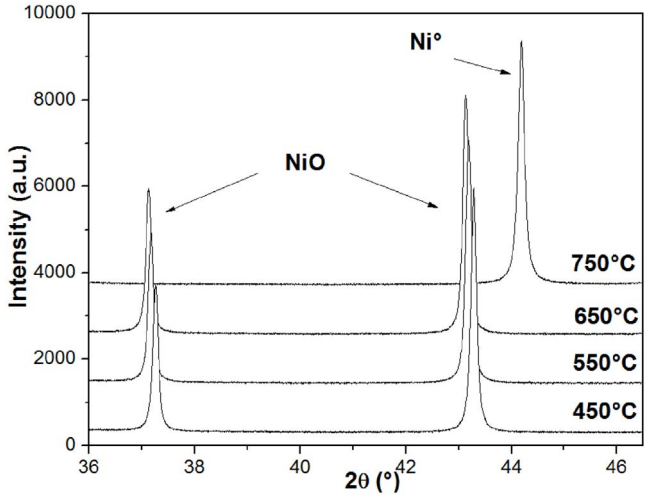


**Fig. 8.** In situ XPD analysis during CPOM over NiO/ZDC without pre-reduction treatment. Feed composition: 2 v/v% $CH_4$ −1 v/v% $O_2$ (He balance).

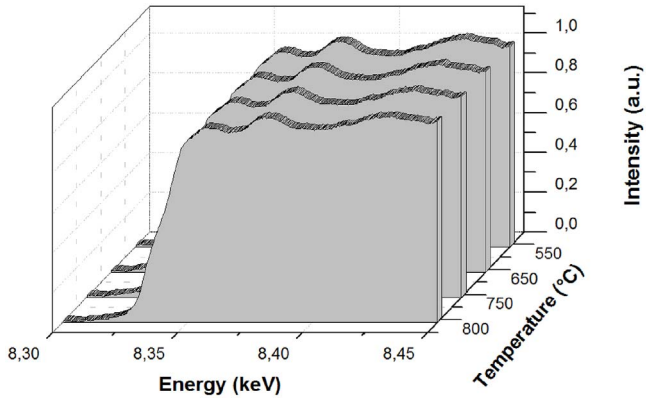


**Fig. 9.** XANES spectra collected at the Ni-K edge during the catalytic tests with pre-reduced NiO/ZDC sample in 2 v/v% $CH_4$ −1 v/v% $O_2$ (He balance).

### 3.3.2. XANES experiments in the Ni K-edge

XANES spectra in the Ni K-edge were collected after the reductive pre-treatment while heating the sample in a flow consisted of 2 v/v% $CH_4$ −1 v/v% $O_2$ (He balance) feed gas flow. The sample was heated at a rate of 10 °C $min^{-1}$ from room temperature to 800 °C, with isothermal steps of 20 min at 550 °C, 650 °C, 750 °C and 800 °C. The spectra collected during reaction conditions are identical to $Ni^0$ standard confirming, through fitting procedure, that nickel is present only as $Ni^0$ (Fig. 9). These results are in good agreement with those observed in XPD analysis (Fig. 7).

### 3.3.3. XANES experiments in the Ce $L_{III}$-edge

Fig. 10(a) shows the XANES spectra collected during heating of sample NiO/ZDC without pre-treatment in 2 v/v% $CH_4$ and 1 v/v% $O_2$ (He balance), from room temperature to 800 °C. In Fig. 10(b) it is shown the spectra collected isothermally at 800 °C in 10 v/v% $CH_4$ (He balance).

Through the fitting procedure explained elsewhere [26] it was possible to obtain the degree of reduction (α) of $Ce^{4+}$ cations. A linear combination of standard spectra was used as fitting method. $Ce(NO_3)_3$ and the initial spectrum for each sample, were used as Ce(III) and Ce (IV) standards, respectively. Fig. 11 shows the degree of reduction of $Ce^{4+}$ cations in sample NiO/ZDC with feed gas compositions of 2 v/v% $CH_4$ and 1 v/v% $O_2$ in He during heating from room temperature to 800 °C. The $Ce^{3+}$ fraction remains low (α = 4%) even at 800 °C. At 800 °C, when oxygen is removed from the feed, the degree of reduction increases abruptly changing from 4% to almost 70% in 50 min, as indicated in the inset of Fig. 11 which represents the degree of reduction of $Ce^{4+}$ cations with feed gas composition of 10 v/v% $CH_4$ in He at T = 800 °C.

The last experiment performed with NiO/ZDC sample in the Ce $L_{III}$-edge, consisted in a strong pre-reduction of the fresh sample, in 5 v/v% $H_2$ in He, from room temperature up to 800 °C. Then, the reactor was purged in He, and the catalytic experiments were performed isothermally at 800 °C. As shown in Fig. 12, the first atmosphere fed to the reactor consisted in 2 v/v% $CH_4$ and 1 v/v% $O_2$ ($CH_4$:$O_2$ = 2), and it was maintained for 40 min. A constant degree of reduction of $Ce^{4+}$ cations was observed (α ~ 85%). Afterwards, the feed $CH_4$:$O_2$ ratio was set equal to 1, and in this condition the degree of reduction of cerium cations started to decrease, evidencing that some reoxidation of $Ce^{3+}$ cations to $Ce^{4+}$ took place. However, after 120 min the degree of reduction still remained above 20% (see Fig. 12).

### 3.4. Mass spectrometry: distribution of reaction products

During XPD and XANES in situ experiments, the outlet line of the reactor was connected to a Pfeiffer QMS 422 Quadrupole Mass Spectrometer, in order to follow the evolution of the distribution of

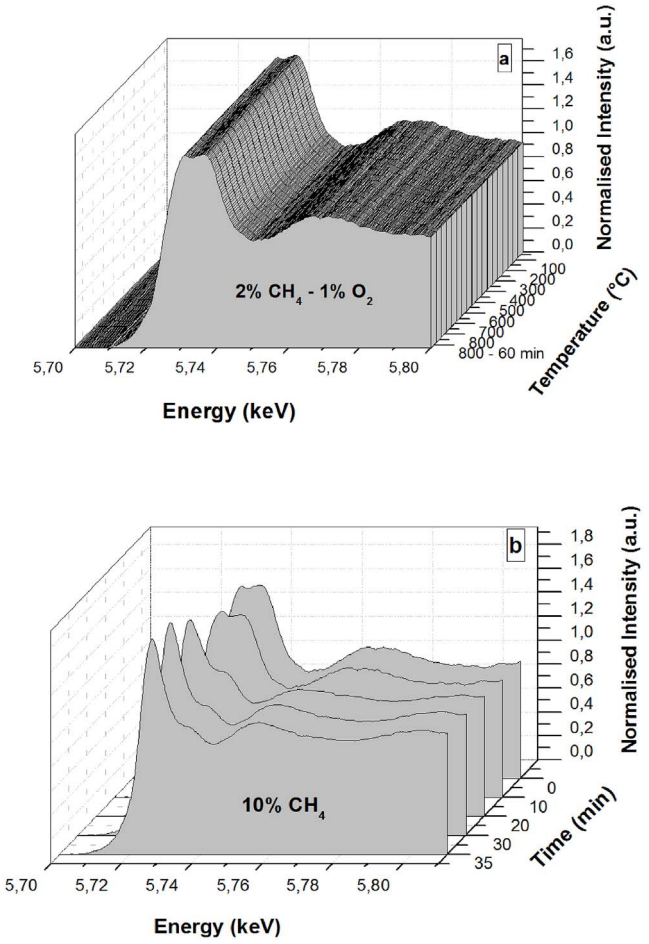


**Fig. 10.** XANES spectra collected in Ce $L_{III}$ absorption edge for sample NiO/ZDC, with feed gas compositions of: (a) 2 v/v% $CH_4$ and 1 v/v% $O_2$ in He during heating from RT to 800 °C; (b) 10 v/v% $CH_4$ in He at T = 800 °C.

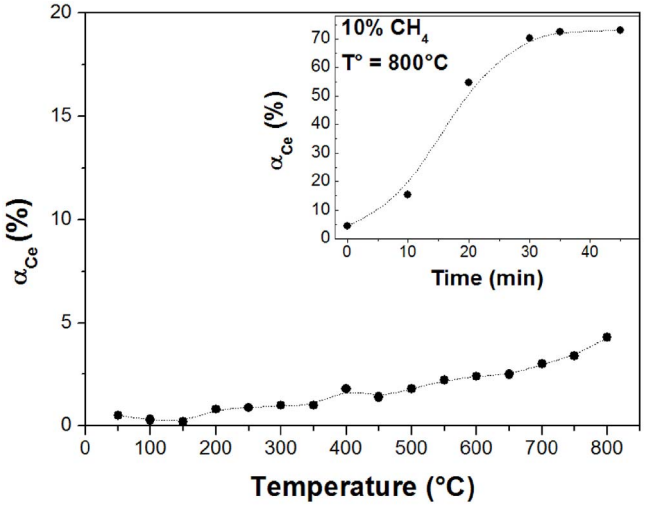


**Fig. 11.** Degree of reduction of $Ce^{4+}$ cations in sample NiO/ZDC with feed gas compositions of: 2 v/v% $CH_4$ and 1 v/v% $O_2$ in He during heating from room temperature to 800 °C; (inset) 10 v/v% $CH_4$ in He at T = 800 °C.

products in different reaction conditions.

Fig. 13 shows mass spectrometry data collected during catalytic tests (CPOM reaction conditions: 2 v/v% $CH_4$ −1 v/v%$O_2$, He balance) performed with the pre-reduced NiO/ZDC catalyst.

During the heating from 550 °C to 650 °C, it was detected a constant increase in total ($CO_2$ and $H_2O$) and partial (CO and $H_2$) oxidation

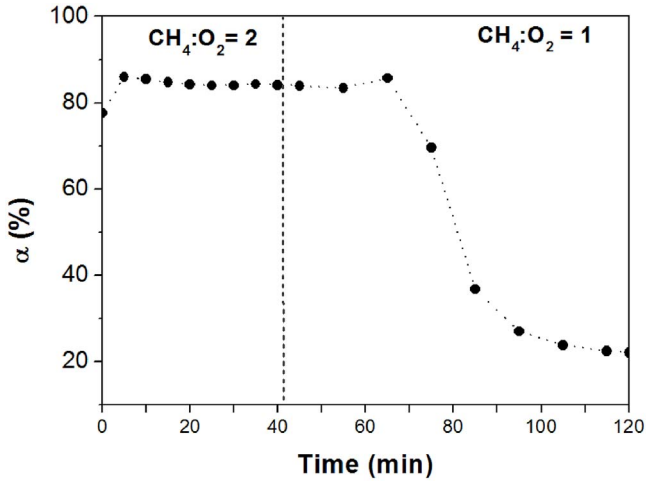


**Fig. 12.** Degree of reduction of $Ce^{4+}$ cations for NiO/ZDC sample pre-reduced at 800 °C, when exposed to different $CH_4$:$O_2$ feed ratio at 800 °C.

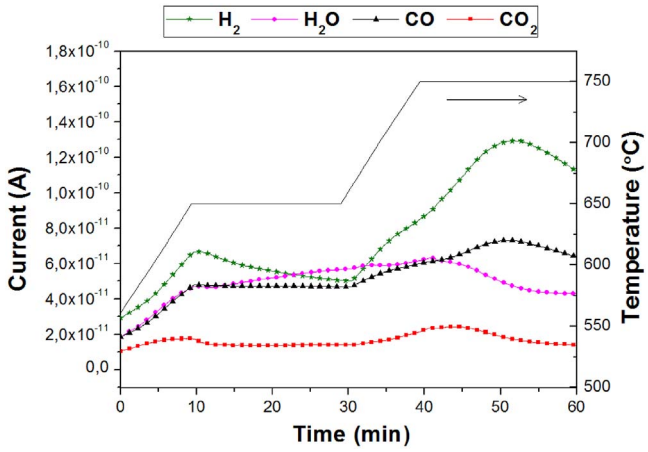


**Fig. 13.** Mass spectrometry data collected in reaction conditions (2%$CH_4$ − 1%$O_2$, He balance) of NiO/ZDC sample with pre-reducing treatment at 550 °C.

products. When the temperature reaches 650 °C, the production of $H_2$ diminishes and the $H_2O$ signal increases, while CO and $CO_2$ signals remain almost constant. According to our previous observation in in-situ XPD and XANES experiments in Ni and Ce edges, at 650 °C it was observed an increment of $Ce^{4+}$ reduction which implies $H_2$ consumption and water production as it is observed in the spectrometer signals. As temperature increases from 650 °C to 750 °C, all the signals of CO, $CO_2$, $H_2$ and $H_2O$ also increase, but it is observed a more markedly change in partial oxidation products (CO and $H_2$). At 750 °C, it is clear the preponderance of methane partial oxidation process evidenced by the increase of $H_2$ and CO signals and the decrease of $CO_2$ and $H_2O$ ones. After 10 min in this condition, all the reaction products begin to decrease, and the catalyst deactivates.

We also analyzed the products distribution when the pre-reduced NiO/ZDC sample is exposed to changes in $CH_4$:$O_2$ ratio at constant temperature (T = 800 °C). When the atmosphere fed to the reactor consisted in 2 v/v% $CH_4$ and 1 v/v% $O_2$, a mixture of CO, $CO_2$, $H_2$ and $H_2O$ was detected in the exit gas (Fig. 14), while a constant degree of reduction of $Ce^{4+}$ cations was observed. Afterwards, the feed $CH_4$:$O_2$ ratio was set equal to 1. In this slightly oxidant condition, it was detected a decrease in the production of CO and $H_2$, with an increase of $CO_2$ and $H_2O$. At the same time, the degree of reduction started to decrease, suggesting that the $Ce^{3+}$ cations were re-oxidized to $Ce^{4+}$. However, after 120 min the degree of reduction still remains above 20%.

When we analyze the data collected in CPOM reaction conditions

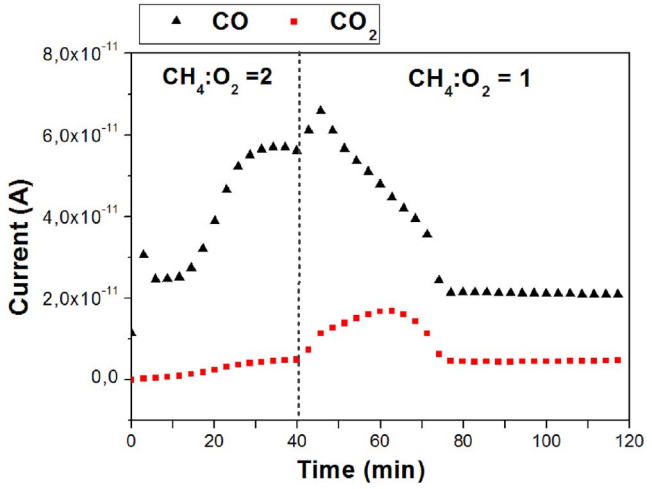


**Fig. 14.** Mass spectrometer signals of CO and $CO_2$ for pre-reduced NiO/ZDC sample when submitted to different $CH_4$:$O_2$ feed ratio at 800 °C.

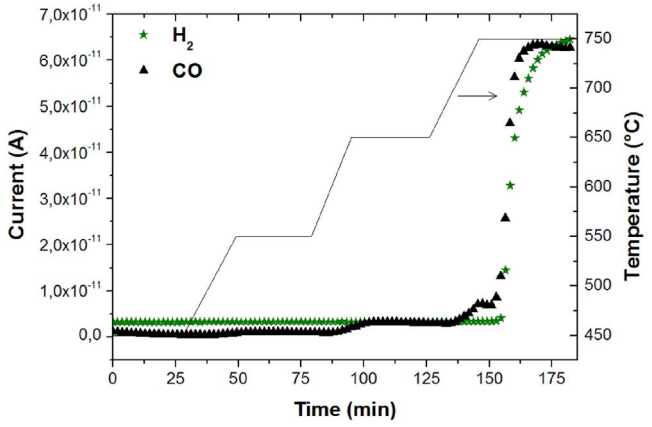


**Fig. 15.** Mass spectrometry currents corresponding to $H_2$ and CO collected in the reactor outlet line during CPOM over NiO/ZDC without pre reduction treatment. Feed composition: 2 v/v% $CH_4$ −1 v/v% $O_2$ (He balance).

(2%$CH_4$ − 1%$O_2$, He balance) over the NiO/ZDC sample without pre-reducing treatment, we can see that the catalyst is almost inactive for CPOM below 650 °C (Fig. 15). Above this temperature $H_2$ and CO signals increases abruptly. The degree of reduction of $Ce^{4+}$ cations remains close to 5% in all the temperature range (Fig. 11). The increase in the partial oxidation products agree with the reduction of NiO to $Ni^0$ observed in XPD analysis (see Fig. 8). From these observations, it can be concluded that $Ni^0$ is necessary to produce the CPOM over NiO/ZDC catalyst. Similar behaviour was observed by other authors for partial oxidation of methane over Ni based catalysts [29–31]. Also, Shan et al. [32] proposed that both $Ni^0$ and $Ce^{3+}$ with oxygen vacancy are the active sites for the CPOM over $Ce_{1-x}Ni_xO_Y$ catalysts. In our work, we found that Ni° is the active centre to produce the partial oxidation of methane. The occurrence of total or partial oxidation of methane is dependent on the feed ratio $CH_4$:$O_2$ and the $Ce^{4+}/Ce^{3+}$ ratio.

The oxidation of methane was also analyzed isothermally at 800 °C, in a feed ratio of $CH_4$:$O_2$ = 2, over NiO/ZDC without pre-treatment. The sample was heated at 10 °C/min up to 800 °C. In Fig. 16, it can be observed that in the first minutes at 800 °C, $CO_2$ and $H_2O$ production show a decrease while CO and $H_2$ signals increase. After a few minutes, CO and $H_2$ signals decrease due to catalyst deactivation. This deactivation is probably due to the formation of carbonaceous deposits, observed in spent catalysts by SEM (Fig. 2c). It is worth to mention that nickel is present in the sample as $Ni^0$.

After 25 min at 800 °C, the composition ratio was changed to $CH_4$:$O_2$ = 1 keeping the temperature constant. In this new stage, a

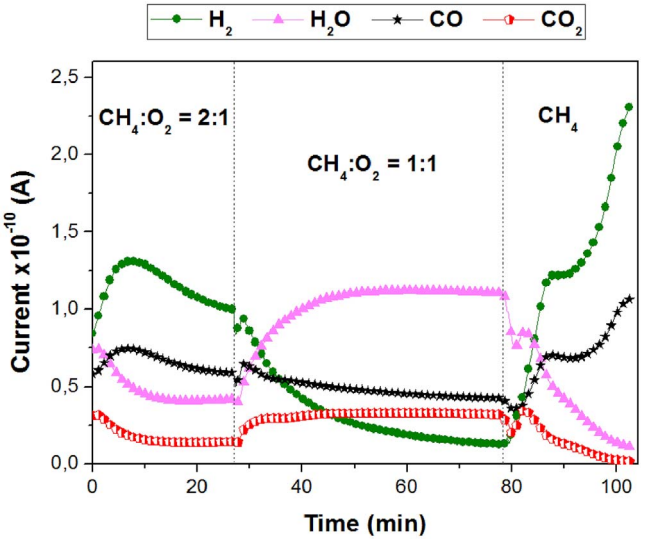


**Fig. 16.** Mass spectrometry data collected in reaction conditions of NiO/ZDC sample without pre-treatment, at T = 800 °C. Feed composition: 2 v/v% $CH_4$ −1 v/v% $O_2$ (He balance).

pronounced increase of $CO_2$ and $H_2O$ was observed, and a decrease of CO and $H_2$, indicating the preponderance of methane total oxidation.

After 50 min in this atmosphere with equimolar composition ($CH_4$:$O_2$ = 1), the oxygen was removed from the feed, establishing an atmosphere of 10%mol $CH_4$ (He balance). The catalyst begins to deliver oxygen from its structure, and in the first minutes the oxygen is enough to produce total oxidation of methane. As time goes by, the oxygen is depleted leading to partial oxidation of methane. At the same time, from XANES experiments in this atmosphere and temperature conditions (Fig. 11) it can be seen that the degree of reduction of $Ce^{4+}$ cations increases, delivering oxygen from the solid structure. As the degree of reduction increases the kinetics of oxygen release slows, leading to the preponderance of CPOM.

### 3.5. Conventional catalytic tests

Preliminary catalytic tests indicate that the inert material employed to dilute the catalytic bed does not affect the results of the experiments.

In Fig. 17(a) we present the methane conversion vs. reaction temperature. At temperatures below 700 °C fresh NiO/ZDC sample behaves like a catalyst for total oxidation, being $CO_2$ and $H_2O$ the only reaction products as it was observed in all the in situ experiments. Above 700 °C the conversion shows an abrupt increase up to 100%, being CO and $H_2$ the main products, with a $H_2$/CO molar ratio of 2. These results are completely similar to those detailed in previous sections (Figs. 13 and 15).

The pre-reduced catalyst exhibit higher catalytic activity and behave as partial oxidation catalyst in all the temperature range, confirming that the presence of Ni° is necessary for the partial oxidation reaction.

In the tests with pre-reduced catalysts, methane conversion at 700 °C was stable for about 30 min. Then the pressure in the catalytic bed significantly increased due to the formation of carbonaceous deposits. This observation is in agreement with the deactivation of the catalyst observed by mass spectrometry results and the formation of carbonaceous deposits detected by SEM. In this sense Gopalakrishnan et al. [33] report that during methane steam reforming over $NiCeZrO_2$, the catalyst with higher NiO particle size evidence formation of carbon patches, while the catalyst with smaller NiO particle size shows stability with time on stream. Also, Xu et al. [34] affirm that for partial oxidation of methane, the deactivation of Ni catalysts is mainly due to the formation of carbonaceous deposits and to active metal sintering. They

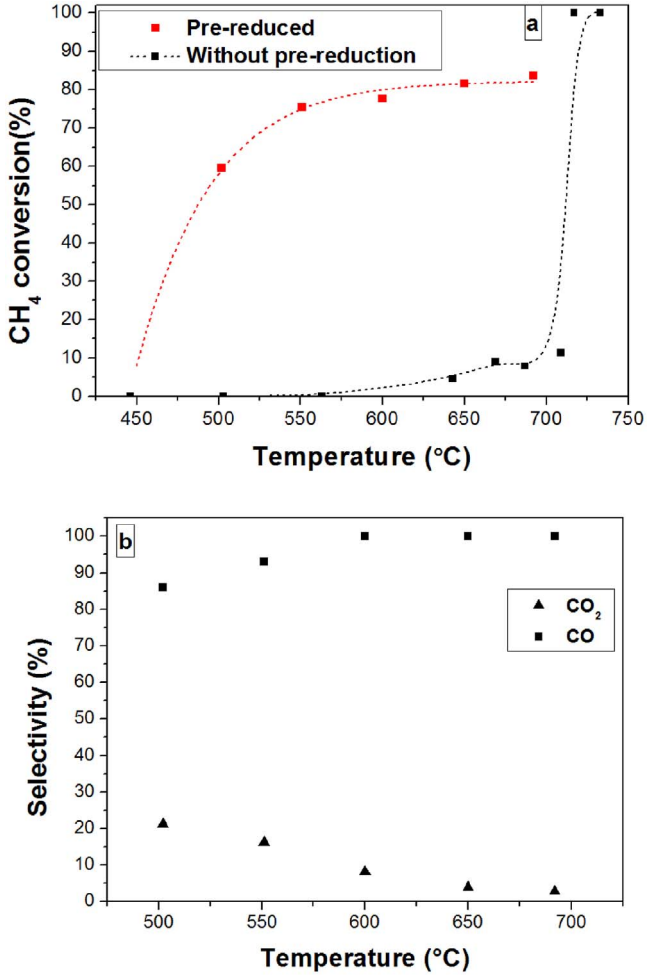


**Fig. 17.** a) Methane conversion vs. reaction temperature for fresh and pre-reduced NiO/ZDC. b) Selectivity to CO and $CO_2$, for pre-reduced NiO/ZDC. Feed composition: 2% $CH_4$, 1% $O_2$ ($N_2$ balance).

studied a series of $Ni/Ce_xZr_{1-x}O_2$ catalysts, and they found that the specific surface area and the Ni surface dispersion are the key factors to improve the coking resistance. We did not observe the formation of carbonaceous deposits in our previous work [20], despite the nickel content (50 wt.%) was close to the value used in this work (60 wt.%). The explanation for this different behaviour should be associated with the different calcination temperature used in both cases. It is well-known that in Ni/ZDC catalysts Ni° particles are very active in dehydrogenation of methane while ZDC support has the ability to rapidly oxidize the dehydrogenated fragments. This last process takes place in the Ni°/ZDC interfaces [12]. The high calcination temperature used in the synthesis of the catalyst studied in the present work reduces the kinetic mechanism of carbon removal via Ni particle sintering. Nevertheless, after regeneration under air flow at 500 °C for a few minutes, the catalysts recovered the original activity and selectivity. On the other hand, at temperatures below 600 °C the catalytic behaviour was stable during a typical work period of 5 h.

## 4. Conclusions

By a multi-technique approach, we analyzed the crystalline structure, catalytic activity, and the oxidation state of metal cations in NiO (60 wt.%)/$Ce_{0.9}Zr_{0.1}O_2$ catalyst under the conditions used in Partial Oxidation of Methane. The ZDC crystallites in the fresh support that was calcined at 600 °C are nanometric. When calcined at 1000 °C the ZDC crystallites grow but keep the nanometric size, confirming that the incorporation of zirconium in the ceria structure disables the growth of crystallites to micrometric sizes. NiO(60 wt.%)/$Ce_{0.9}Zr_{0.1}O_2$ is an active catalyst for CPOM reaction, evidencing total conversion of methane to synthesis gas above 700 °C. Through in-situ XANES studies, it was determined that nickel is totally reduced in reaction conditions leading to total conversion of methane to synthesis gas, and cerium cations are partially reduced with a very low level of reduction (below 5%). In situ XPD and XANES experiments confirmed that Ni° is the active centre to produce the partial oxidation of methane. By means of mass spectrometry data, it was verified the consistence of this results with those obtained through conventional catalytic tests performed in fixed-bed reactor. Besides, in-situ XANES at Ce-$L_{III}$ confirmed that cerium cations are responsible for providing lattice oxygen to form $CO_x$ mixtures. The occurrence of total or partial oxidation of methane is dependent on the feed ratio $CH_4$:$O_2$ and related to $Ce^{4+}/Ce^{3+}$ ratio. The results obtaining in this work can help to tailor the catalyst and the reaction conditions in order to obtain a better catalytic performance.

## Acknowledgements

This work was supported by the Brazilian Synchrotron Light Laboratory (LNLS) under proposals D06A-DXAS-9949 and XRD1-14413, Agencia Nacional de Promoción Científica y Tecnológica (Argentina, PICT 2013 N°1493, 1032 and 1587), and CONICET (Argentina, PIP 112 2013 0100151 CO).

## References

[1] S. Zinoviev, F. Muller-Langer, P. Das, N. Bertero, P. Fornasiero, M. Kaltschmitt, G. Centi, S. Miertus, ChemSusChem 3 (2010) 1106–1133.
[2] N.S. Lewis, D.G. Nocera, Proc. Natl. Acad. Sci. U. S. A. 103 (2006) 15729–15735.
[3] A.B. Stambouli, E. Traversa, Renew. Sustain. Energy Rev. 6 (2002) 433–455.
[4] D.A. Hickman, L.D. Schmidt, J. Catal. 13 (1992) 267–282.
[5] D.A. Hickman, E.A. Haupfear, L.D. Schmidt, Catal. Lett. 17 (1993) 223–237.
[6] E.P.J. Mallens, J.H.B.J. Hoebink, G.B. Marin, J. Catal. 167 (1997) 43–53.
[7] S. Eriksson, S. Rojas, M. Boutonnet, J.L.G. Fierro, Appl. Catal. A: Gen. 326 (2007) 8–16.
[8] V.A. Sadykov, N.N. Sazonova, A.S. Bobin, V.S. Muzykantov, E.L. Gubanova, G.M. Alikina, A.I. Lukashevich, V.A. Rogov, E.N. Ermakova, E.M. Sadovskaya, N.V. Mezentseva, E.G. Zevak, S.A. Veniaminov, M. Muhler, C. Mirodatos, Y. Schuurman, A.C. van Veen, Catal. Today 169 (2011) 125–137.
[9] L.M.T.S. Rodrigues, R.B. Silva, M.G.C. Rocha, P. Bargiela, F.B. Noronha, S.T. Brandao, Catal. Today 197 (2012) 137–143.
[10] Wen-Sheng Dong, Ki-Won Jun, Hyun-Seog Roh, Zhong-Wen Liu, Sang-Eon Park, Catal. Lett. 78 (2002) 215–222.
[11] M. Salazar-Villalpando, B. Reyes, Int. J. Hydrogen Energy 34 (2009) 9723–9729.
[12] D.H. Prasad, H.-Y. Jung, H.-G. Jung, B.-K. Kim, H.-W. Lee, J.-H. Lee, Mater. Lett. 62 (2008) 587–590.
[13] W. Dong, K. Jun, H. Roh, Z.-W. Liu, S.-E. Park, Catal. Lett. 78 (2002) 215–222.
[14] B. Enger, R. Lodeng, A. Holmen, Appl. Catal. A 346 (2008) 1–27.
[15] Provas Pal, Rajib Kumar Singha, Arka Saha, Rajaram Bal, Asit Baran Panda, J. Phys. Chem. C 119–124 (2015) 13610–13618.
[16] P. Fornasiero, R. Dimonte, G. Ranga Rao, J. Kaspar, S. Meriani, A. Trovarelli, M. Graziani, J. Catal. 151 (1995) 168–177.
[17] Susana Larrondo, María Adelina Vidal, Beatriz Irigoyen, Aldo F. Craievich, Diego G. Lamas, Ismael O. Fábregas, Gustavo E. Lascalea, Noemí E. Walsöe de Reca, Norma Amadeo, Catal. Today 107–108 (2005) 53–59.
[18] S.A. Larrondo, A. Kodjaian, I. Fábregas, M.G. Zimicz, D.G. Lamas, B.E. Walsöe de Reca, N.E. Amadeo, Int. J. Hydrogen Energy 33 (2008) 3607–3613.
[19] G. Pantaleo, V. La Parola, F. Deganello, R.K. Singha, R. Bal, A.M. Venezia, Appl. Catal. B: Environ. 189 (2016) 233–241.
[20] S.A. Larrondo, A. Kodjaian, I. Fábregas, M.G. Zimicz, D.G. Lamas, N.E. Walsöe de Reca, N.E. Amadeo, Int. J. Hydrogen Energy 33 (2008) 3607–3613.
[21] L.M. Toscani, M.G. Zimicz, J.R. Casanova, S.A. Larrondo, Int. J. Hydrogen Energy 39 (2014) 8759–8766.
[22] M.G. Zimicz, P. Núñez, J.C. Ruiz Morales, D.G. Lamas, S.A. Larrondo, J. Power Sources 238 (2013) 87–94.
[23] J.C. Ruiz Morales, et al., Pilas de combustible de óxidos sólidos: SOFC, Centro de la Cultura Popular Canaria (Ed.) Tenerife, España, 2008.
[24] M.G. Zimicz, I.O. Fábregas, D.G. Lamas, S.A. Larrondo, Mater. Res. Bull. 46 (2011) 850–857.
[25] J. Rodríguez-Carvajal, Fullprof: a Program for Rietveld Refinement and Profile Matching Analysis of Complex Powder Diffraction Patterns, Laboratoire Léon Brillouin (CEA-CNRS).
[26] M.G. Zimicz, S.A. Larrondo, R.J. Prado, D.G. Lamas, Int. J. Hydrogen Energy 37 (2012) 14881–14886.
[27] J.A. Rodríguez, J.C. Hanson, A.I. Frenkel, J.Y. Kim, M. Pérez, J. Am. Chem. Soc. 124

(2) (2002) 346–354.
[28] R.D. Shannon, C.T. Prewitt, Acta Crystallogr. B 25 (1969) 925–1048.
[29] L.M.T.S. Rodrigues, R.B. Silva, M.G.C. Rocha, P. Bargiela, F.B. Noronha, S.T. Brandão, Catal. Today 197 (2012) 137–143.
[30] D. Dissanayake, M.P. Rosynek, K.C.C. Kharas, J.H. Lunsford, J. Catal. 132 (1991) 117–127.
[31] J. Requies, M.A. Cabrero, V.L. Barrio, M.B. Güemez, J.F. Cambra, P.L. Arias, F.J. Pérez-Alonso, M. Ojeda, M.A. Peña, J.L.G. Fierro, Appl. Catal. A: Gen. 289 (2) (2005) 214–223.
[32] W. Shan, M. Fleys, F. Lapicque, D. Swierczynski, A. Kiennemann, Y. Simon, P.M. Marquaire, Appl. Catal. A: Gen. 311 (2006) 24–33.
[33] S. Gopalakrishnan, M.G. Faga, I. Miletto, S. Coluccia, G. Caputo, S. Sau, A. Giaconia, G. Berlier, Appl. Catal. B: Environ. 138–139 (2013) 353–361.
[34] S. Xu, X. Wang, Fuel 84 (2005) 563–567.